

# Water Resources Research<sup>®</sup>



## RESEARCH ARTICLE

10.1029/2022WR032225

†Deceased.

### Key Points:

- Plum Island mesotidal marsh system adapts itself to most of the sea-level rise (SLR) scenarios but will undergo changes in vegetation type
- Lower SLR scenarios are favorable for Plum Island estuary marsh productivity but higher SLR results in low marsh dominance, mudflat creation, and migration
- Integrated modeling that couples biological feedbacks and hydrodynamics is critical to capture flow dynamics

### Correspondence to:

K. Alizad,  
[Alizad@sc.edu](mailto:Alizad@sc.edu)

### Citation:

Alizad, K., Morris, J. T., Bilskie, M. V., Passeri, D. L., & Hagen, S. C. (2022). Integrated modeling of dynamic marsh feedbacks and evolution under sea-level rise in a mesotidal estuary (Plum Island, MA, USA). *Water Resources Research*, 58, e2022WR032225. <https://doi.org/10.1029/2022WR032225>

Received 19 FEB 2022

Accepted 23 JUL 2022

### Author Contributions:

**Conceptualization:** Karim Alizad, James T. Morris, Scott C. Hagen

**Formal analysis:** Karim Alizad, James T. Morris, Matthew V. Bilskie, Scott C. Hagen


**Funding acquisition:** James T. Morris, Davina L. Passeri, Scott C. Hagen

**Investigation:** Karim Alizad, James T. Morris, Matthew V. Bilskie, Scott C. Hagen

© 2022 The Authors. This article has been contributed to by U.S. Government employees and their work is in the public domain in the USA.

This is an open access article under the terms of the [Creative Commons Attribution-NonCommercial-NoDerivs License](https://creativecommons.org/licenses/by/4.0/), which permits use and distribution in any medium, provided the original work is properly cited, the use is non-commercial and no modifications or adaptations are made.

## Integrated Modeling of Dynamic Marsh Feedbacks and Evolution Under Sea-Level Rise in a Mesotidal Estuary (Plum Island, MA, USA)

Karim Alizad<sup>1,2</sup> , James T. Morris<sup>3</sup> , Matthew V. Bilskie<sup>4</sup> , Davina L. Passeri<sup>5</sup> , and Scott C. Hagen<sup>6†</sup>

<sup>1</sup>Baruch Institute for Marine and Coastal Sciences, University of South Carolina, Columbia, SC, USA, <sup>2</sup>St. Petersburg Coastal and Marine Science Center Contractor, U.S. Geological Survey, St. Petersburg, FL, USA, <sup>3</sup>University of South Carolina, Columbia, SC, USA, <sup>4</sup>University of Georgia, Athens, GA, USA, <sup>5</sup>U.S. Geological Survey, St. Petersburg, FL, USA, <sup>6</sup>Louisiana State University, Baton Rouge, LA, USA

**Abstract** Around the world, wetland vulnerability to sea-level rise (SLR) depends on different factors including tidal regimes, topography, creeks and estuary geometry, sediment availability, vegetation type, etc. The Plum Island estuary (PIE) is a mesotidal wetland system on the east coast of the United States. This research applied a newly updated Hydro-MEM (integrated hydrodynamic-marsh) model to assess the impacts of intermediate-low (50 cm), intermediate (1 m), and intermediate-high (1.5 m) SLR on marsh evolution by the year 2100. Model advancements include capturing vegetation change, inorganic and below and aboveground organic matter portion of marsh platform accretion, and mudflat creation. Although the results indicate a low vulnerability marsh at the PIE, the vegetation changes from high to low marsh under all SLR scenarios (2%–22%), with the higher bounds belonging to higher rise scenarios. Lower SLR produces more productive marsh (13% gain in high productivity regions), whereas the highest SLR scenario causes increased tidal inundation, which leads to loss in productivity (12% change from high to low productivity regions), generation of mudflats (17% of the domain land), and marsh migration to higher lands. Sensitive nonlinear tidal flow changes, which may be increased or decreased with SLR as a result of mudflat creation, marsh migration, and bottom friction change, emphasize the importance of integrated modeling approaches that include dynamic marsh feedbacks in hydrodynamic modeling and varying hydrodynamic effects on the marsh system.

## 1. Introduction

Coastal marshes provide an abundance of ecological resources, such as habitat and food for many species that benefit coastal economies (Daiber, 1977; Penning & Bertness, 2001; Rozas et al., 2005; Yoskowitz et al., 2017). Marshes also protect shorelines by dissipating waves and attenuating storm surges (Barbier et al., 2013; Costanza et al., 2008), purify coastal water by absorbing chemicals (Jansson et al., 1994; Kadlec, 1999), and store carbon (Forbrich et al., 2018). Research shows that these unique systems are at risk globally and vulnerable to collapse due to sea-level rise (SLR) and climate change (Alizad, Hagen, Morris, Medeiros, et al., 2016; Crosby et al., 2016; Osland et al., 2017; Reed, 1995). How a marsh responds to external stressors is dependent on factors including marsh platform topography, sediment availability, wave erosion, salinity change, nutrient composition, available land for migration, species type, and tidal regimes (Alizad et al., 2018; Foster-Martinez et al., 2020; Raposa et al., 2016).

Tidal regimes play an essential role in the response of salt marshes to a rise in sea level. Tidal regimes are defined by their tide range, which is the absolute value between the average of high tides (mean high water [MHW]), and the average of low tides (mean low water [MLW]). Marsh systems are more sensitive to SLR in microtidal systems (<2 m tide range) than mesotidal (2–4 m) or macrotidal (>4 m) systems (Friedrichs & Perry, 2001; Kirwan & Guntenspergen, 2010). SLR also has the potential to increase tidal ranges in coastal bays and estuaries and can alter flood or ebb dominance and resulting sediment transport in the system (Jiang et al., 2020; Passeri et al., 2016). These nonlinear SLR-induced changes can affect many species' ecological habitats, including wetlands, forest regions, mudflats, and barrier islands.

Although marshes maintain or move toward equilibrium with mean sea level (MSL) by trapping sediment and organic matter (Morris et al., 2002; Mudd et al., 2009), the projected increasing rate of SLR (Parris et al., 2012;

**Methodology:** Karim Alizad, James T. Morris, Matthew V. Bilskie, Scott C. Hagen

**Resources:** Davina L. Passeri, Scott C. Hagen

**Supervision:** Karim Alizad, James T. Morris, Davina L. Passeri, Scott C. Hagen

**Validation:** Karim Alizad, Matthew V. Bilskie

**Visualization:** Karim Alizad, Matthew V. Bilskie

**Writing – original draft:** Karim Alizad

**Writing – review & editing:** Karim Alizad, James T. Morris, Matthew V. Bilskie, Davina L. Passeri, Scott C. Hagen

Sweet et al., 2017) attracts more attention to these unique ecological systems due to the amount of recent global marsh coverage loss (Crosby et al., 2016). Natural resource officials manage their land in part based on guidance from scientists to restore and increase the resiliency of marshes, including data from integrated wetland models (Wigand et al., 2017). The latest integrated wetland models include physical and biological feedback processes through tidal hydrodynamics and ecological processes (Alizad, Hagen, Morris, Bacopoulos, et al., 2016; D'Alpaos et al., 2007; Fagherazzi et al., 2012; Hagen et al., 2013; Kirwan & Murray, 2007). It is critical to include the dynamic effects of SLR such as nonuniform water level changes in the bays and creeks and incorporate them into marsh models (Passeri et al., 2015). This connection between hydrodynamic and marsh models helps to assess how a marsh responds to variations in tidal hydrodynamics, and in turn, how vegetation adjustments, mudflat creation, and upland migration can impact hydrodynamics. Hydro-MEM couples a hydrodynamic and biological model to simulate the effects of SLR and wetland system dynamics and their interconnections in a feedback process (Alizad, Hagen, Morris, Bacopoulos, et al., 2016). Hydro-MEM takes various hydrodynamic inputs and experimental factors for belowground and aboveground biomass, suspended sediment, compaction, root-shoot ratio, and other marsh platform accretion modeling in response to SLR and provides marsh productivity, vegetation type, and upland migration possibility, as well as accreted marsh platform elevation. Hydro-MEM has been applied for several estuarine systems in the United States to assess the impacts of SLR on marsh systems to provide restoration information and guidance to coastal managers and inputs to other models such as storm surge or wave attenuation (Alizad, Hagen, Morris, Medeiros, et al., 2016; Alizad et al., 2018; Bacopoulos et al., 2019; Bilskie et al., 2016; Foster-Martinez et al., 2020; Kidwell et al., 2017).

Hydro-MEM is employed to investigate the response of a mesotidal marsh system (Plum Island estuary–PIE) in the northeast United States. In particular, this manuscript aims to introduce a high resolution hydrodynamic model for PIE and assess this mesotidal marsh system productivity and vegetation type, and its vulnerability to SLR. The other main goal of this research paper is to investigate the need for the coupled models incorporating the feedback process between hydrodynamics and marsh models in long-term marsh projections by analyzing any landscape-driven flow variation.

## 2. Methods

### 2.1. Study Site

PIE, located in the northeastern coastline of Massachusetts (Figure 1a), is an ebb-dominated estuary covered mainly by high marsh (*Spartina patens*) due to its topography, geometry, and mesotidal regime; the low marsh found in low lands of the system is dominated by *Spartina alterniflora*. This estuary was selected for this study due to long-term data availability for building a robust model since it is a part of the National Science Foundation (NSF) Long-Term Ecological Research (LTER) study. The estuary and tidal wetlands were formed between 2,500 and 3,500 years ago, and deforestation between eighteen and nineteenth centuries transported large amounts of sediment from upland areas (Kirwan et al., 2011). Presently, it is one of the largest remaining marsh-dominated estuaries in the northeast United States (Hopkinson et al., 2018; Kirwan et al., 2011). Previous studies have concluded that most sediment accreted on the marsh platform is redistributed from marsh edge erosion, with a small amount being deposited from uplands (Hopkinson et al., 2018). PIE tides are semidiurnal with an average range of 2.9 m, and marshes are flooded during spring tides with the neap-spring range of 2.6–3.6 m (Morris et al., 2013; Vallino & Hopkinson, 1998). The mean depth of the estuary from the mouth to the head ranges from about 4.7 to 1.4 m. Average annual discharge from the watershed to the estuary is  $11 \text{ m}^3 \text{ s}^{-1}$ ; the volume of water is about 67 times lower than a single tidal prism, meaning the river inflow is very small compared to the tidal flow (Vallino & Hopkinson, 1998). About  $39.8 \text{ km}^2$  of the  $59.8 \text{ km}^2$  estuary is covered by wetlands (Buchsbaum et al., 2009).

The high marsh is flooded less frequently and receives less sediment and organic matter than the low marsh regions (Schmitt et al., 1998). The National Oceanic and Atmospheric Administration (NOAA) tide gauge in Boston, MA (gauge#8443970) shows a SLR trend of  $2.87 \pm 0.15 \text{ mm yr}^{-1}$ , which can favor the marsh system and increase its productivity if SLR continues with the same trend. A field experiment assessing bioassay and marsh organ curves in PIE indicated positive response of marshes to fertilization. It is expected that *S. alterniflora* (low marsh) will increase as the first response of PIE to SLR even with the current rising rate (Morris et al., 2013). In this study, three projections of SLR for the year 2100 were used to assess changes in hydrodynamics and resulting

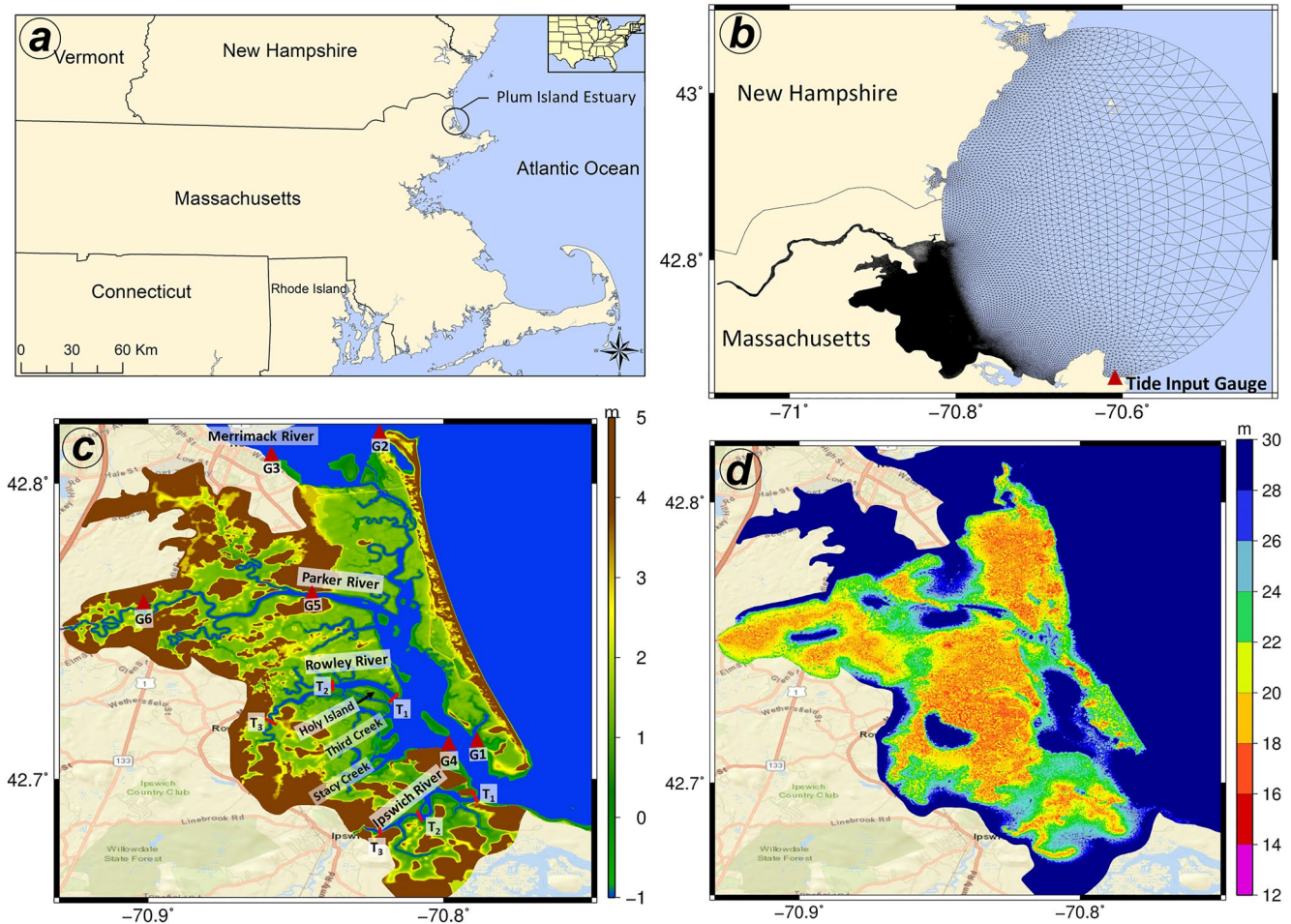


**Figure 1.** (a) Plum Island Estuary location in the United States. (b) Advanced CIRCulation model (ADCIRC) unstructured mesh. (c) Topography and bathymetry (m, NAVD88) as described by the ADCIRC mesh along with rivers, three transects of  $T_1$  (inlet),  $T_2$  (middle),  $T_3$  (upland) on Ipswich and Rowley Rivers, and gauge station (G1 to G6) locations. (d) Unstructured mesh resolution (m).

vegetation change (Figure 2): intermediate-low (0.5 m), intermediate (1 m), and intermediate-high (1.5 m) (Sweet et al., 2017).

## 2.2. Hydro-MEM Wetland Model

To include the SLR-induced hydrodynamic variations in the marsh system dynamics, as well as biological feedbacks in the PIE mesotidal wetland, the integrated Hydro-MEM model was used. This model is a coupled hydrodynamic (ADvanced CIRCulation model) and marsh model (MEM) that simulates the hydrodynamic and biological interconnections of a salt marsh system (Alizad, Hagen, Morris, Bacopoulos, et al., 2016). This model has a time-stepping feedback loop that starts with a hydrodynamic model, which runs for a full tidal cycle with time step of a second and provides input in the form of tidal datums for MEM. MEM outputs the accretion rate and marsh productivity, which are used by Hydro-MEM to update the inputs for the next time step (which is 5–10 years) of the hydrodynamic model. These updated inputs are marsh platform elevation (from the accretion rate output of MEM), bottom friction (from the marsh productivity output of MEM as an indication of roughness), and SLR derived from the NOAA projections (Figure 2). The spatial scale of the model is between 10 and 20 m in the marsh system. Hydro-MEM has been successfully applied to several microtidal estuaries, validated with wetland coverage data, and has been used by several governmental agencies for restoration and management guidance (Alizad, Hagen, Morris, Medeiros, et al., 2016; Alizad et al., 2018). The latest version of Hydro-MEM used in this research accounts for the conversion of marsh to mudflat and marsh species changes (see Section 2.2.3). The main inputs for Hydro-MEM hydrodynamic simulations are topography, bathymetry,



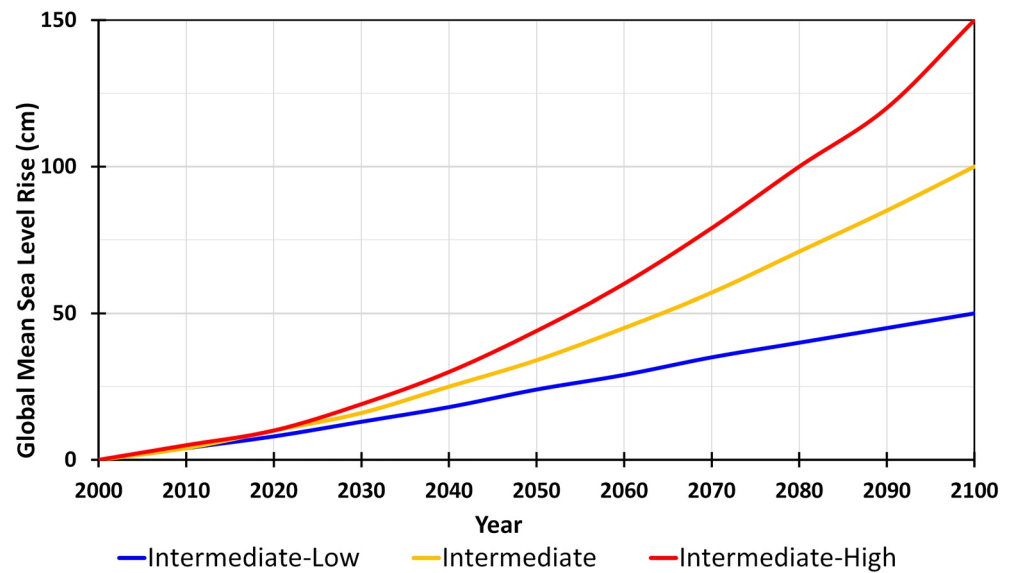


**Figure 2.** Global mean sea level rise (SLR) scenarios derived from Sweet et al. (2017).

shoreline and tidal creek geometry, astronomic tidal forcing, and bottom friction. Outputs from the hydrodynamic simulation that are in the marsh module are MLW, MHW, and MSL.

### 2.2.1. Topography and Bathymetry

Bathymetry was obtained from a previously generated high-resolution data set based on GPS depth and NOAA hydrographic surveys that were used for the PIE LTER FVCOM-based model (Zhao et al., 2010). Topographic information was gathered from the latest lidar-derived 2011 northeast 1 m Digital Elevation Model (DEM) published in August 2013 (OCM Partners, 2020). The lidar was collected with a target ground sample distance of 1 m or better for Massachusetts and resulted in a reported bare-earth root mean square error (RMSE) of 0.071 m based on a set of calibration (ground truth) points, which is sufficient for marsh modeling (Alizad, Medeiros, Foster-Martinez, & Hagen, 2020; K. Alizad, Medeiros, Morris, & Hagen, 2020). The bathymetric and topographic datasets were merged at the shoreline (0 m NAVD88 contour) to form a seamless digital elevation with a spatial resolution of 2 m.

### 2.2.2. Hydrodynamic Model

The hydrodynamic portion of the coupled model simulates water surface elevation and depth-averaged velocity using ADCIRC, which is a two-dimensional, depth-averaged, shallow water hydrodynamic-based code (Luettich & Westerink, 2006). The unstructured model mesh (312,158 nodes and 621,448 elements) extends ~30 km offshore of the mainland. It includes the entirety of PIE, including Plum Island Sound, Parker River, and Merrimack River, with high resolution (15–40 m elements) focused across the salt marsh surface and tidal creeks (Figures 1b and 1d). The seamless bathymetric and topographic DEM elevations were interpolated onto the unstructured mesh nodes using cell area averaging with a 2× smoothing function to reduce sub-grid scale microtopography (Figure 1c) (Bilskie & Hagen, 2013). The model was forced with amplitudes and phases from the eleven dominant offshore astronomic tidal constituents for this region (Q1, O1, P1, K1, N2, M2, S2, K2, NU2, 2N2, and M4). The tidal forcings for these constituents were obtained from the Rockport Harbor NOAA NOS tide gauge (8441551) (Figure 1b). The model includes wetting and drying with a wetting threshold of 10 cm and runs with a 0.5-s time-step. Meteorological forcing was not included.

Two validation runs were performed, and model results were compared to measured water level data. Because we are considering long-term (decadal to century-scale) evolution, short-term perturbations such as meteorological forcings (e.g., winds) that may temporarily change water levels were ignored, and only changes to the tidally-driven components were considered. A 120-day astronomic tide simulation was conducted that began with a 15-day ramp followed by 15-day of dynamic steady state. The simulated water levels over the last 90 days (30–120) were harmonically analyzed over a 14-day period incorporating the least square method (Boon III and

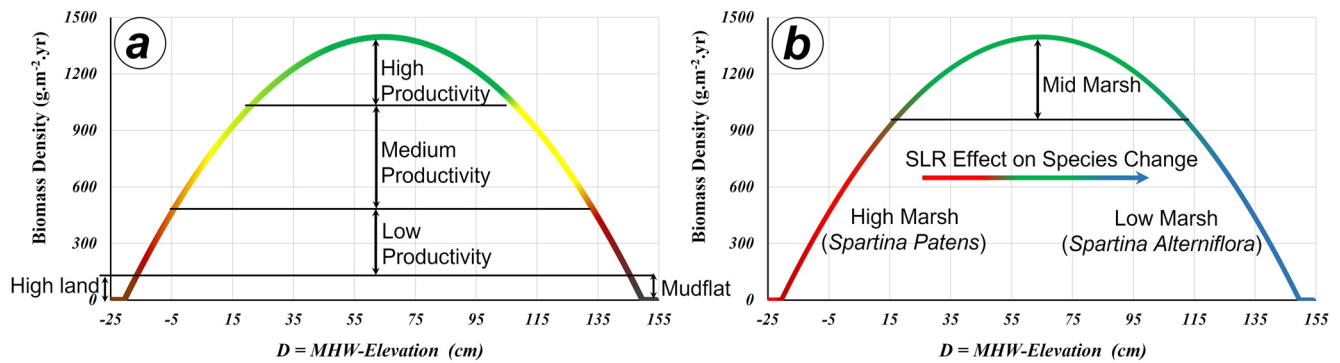


**Figure 3.** Biomass density parabola distribution represents both *Spartina alterniflora* and *Spartina patens* with different color code categorizations for postprocessing the results.  $D$  in the  $x$ -axis represents the relative depth below mean high water and the vertical axis is the biomass density of the plant.

Kiley, 1978) at three NOAA NOS tide gauge stations (Figure 1c, gauges G1, G2, G3). Simulated MHW and MLW at the three NOS tide gauges were compared to gauge-measured MHW and MLW values. The second validation run was set up to compare time-series water levels at three gauges located within the PIE system from 20–30 April 2002 (see Figure 1c for station locations G4, G5, and G6) to measured water levels (derived from a YSI 6600 water quality sonde available through the LTER).

### 2.2.3. Marsh Equilibrium Model Module

The Marsh Equilibrium Model (MEM) module of Hydro-MEM applies an empirical relation between marsh productivity and elevation derived from field experiments using marsh organs (Morris et al., 2013) for this region. The updated formulation of the biomass density ( $B$ ) parabolic curve is  $B = aD + bD^2 + c$  (Figure 3a), where  $D$  is the relative depth and is defined as the difference between MHW and marsh platform elevation from NAVD88 datum ( $D = \text{MHW} - z$ ) in cm and the constants  $a$ ,  $b$ , and  $c$  are  $24.9 \text{ g cm}^{-3} \text{ yr}^{-1}$ ,  $-0.193 \text{ g cm}^{-4} \text{ yr}^{-1}$ , and  $592.7 \text{ g cm}^{-2} \text{ yr}^{-1}$ , respectively. These constants represent a composite of *S. alterniflora* and *S. patens*. The marsh platform accretion formulation (cm/yr) was updated by incorporating the latest version of MEM. It calculates total soil volume change as the sum of both organic and inorganic inputs as  $dz/dt_{\text{total}} = dz/dt_{\text{inorganic}} + dz/dt_{\text{organic}}$  (Morris et al., 2016). The inorganic or mineral contribution is based on Krone (1987) methodology and is as follows:

$$\left(\frac{dz}{dt}\right)_{\text{inorganic}} = \frac{q \times m \times \frac{D}{2} \times \text{IT}}{\text{BD}_i}$$

where  $dz/dt$  is the change in elevation (cm/yr),  $q$  is the capture coefficient of 2.8 and is unitless;  $m$  ( $\text{g/cm}^3$ ) is the suspended sediment concentration (TSS) with median total TSS observations in PIE ranging from less than 10 mg/L at the head and mouth of the estuary to 30–40 mg/L within the estuarine turbidity maximum during spring and fall. The median TSS concentration over space and time was 15.6 mg/L (Hopkinson et al., 2018);  $D$  is the relative depth below mean high water (MHW- $z$ ) in cm. IT is the fractional inundation time calculated as  $(\text{MHW} - z)/(\text{MHW} - \text{MLW})$ , and  $\text{BD}_i$  is the self-packing density of inorganic material ( $=1.99 \text{ g/cm}^3$ ). In addition to the sediment contribution, the organic matter produced can be defined as

$$\left(\frac{dz}{dt}\right)_{\text{organic}} = \frac{k_r \times B}{\text{BD}_o}$$

where  $B$  is the peak standing biomass in a given year ( $\text{g/cm}^2$ ) and  $\text{BD}_o$ , the self-packing density of organic material ( $=0.085 \text{ g/cm}^3$ , (Morris et al., 2016)).  $kr$  ( $=k_r \cdot T_r \cdot R:S$ ) is the refractory or non-decomposing fraction of belowground biomass to its turnover rate and the root-shoot ratio. Root-shoot ratios (R:S) for *S. alterniflora* are typically about 2 (Darby & Turner, 2008). The term “root” in this ratio includes both roots and rhizomes in a ratio of about 1:1 (Darby & Turner, 2008). Morris (1982) model shows an R:S of  $1.5 \pm 0.5$  that depends on light and nutrient treatment. A turnover rate ( $T_r$ ) for the combined root plus rhizome biomass considering that rhizomes are perennial organs with slow turnover is about 1/yr. The refractory fraction ( $k$ ) of this turnover material is proportional to the lignin concentration (Morris et al., 2013) and is approximately 10% of the live dry weight of the

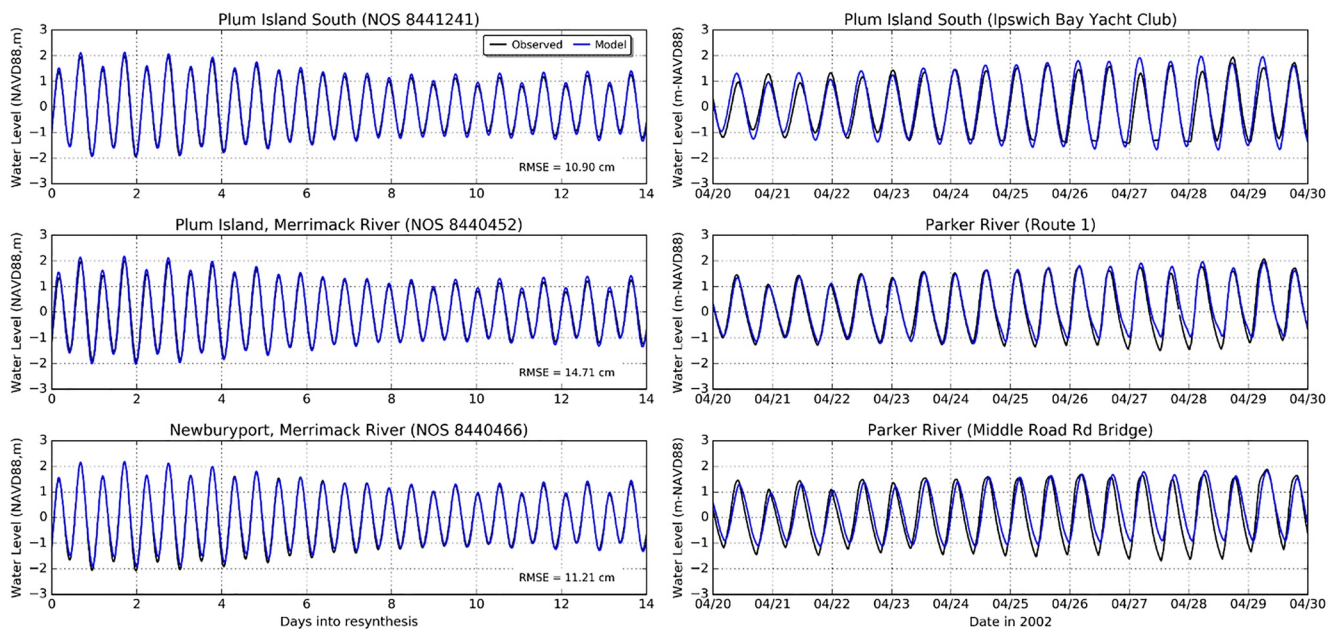


**Figure 4.** Time-series hydrograph of observed (black) and modeled (blue) resynthesized water levels at the three National Oceanic and Atmospheric Administration (NOAA) tide gauges (left—G1, G2, and G3 from top to bottom shown in Figure 1c). Time-series hydrograph of observed and modeled water levels during April 2002 (right—G4, G5, and G6 from top to bottom shown in Figure 1c).

plant (Buth & Voeselek, 1987; Hodson et al., 1984; Wilson et al., 1986). Therefore,  $k_r$  will be calculated as 0.2 ( $=k_r T_p R:S = 0.2$ ). Dividing by  $BD_o$ , the volume of new refractory organic production equivalent to the change in elevation in cm is calculated. Parameters  $D$  and  $IT$  are dependent to hydrodynamic model and are spatially varying, as well as biomass density  $B$ , but the rest are constant and field-related parameters derived for this specific estuary.

The modeled biomass density output was categorized as low, medium, and high productivity, high land, and mudflat regions. Figure 3a displays how the parabola is divided into three main regions of productivity colored in red, yellow, and green; the terminus of the right side of the curve is colored in gray, indicating regions where low productivity marshes are converted into mudflats. The updates to the Hydro-MEM code contain postprocessing steps to categorize marsh species into the low and high marsh regions and a mid-marsh between high and low marsh (Figure 3b). Results that assess SLR scenarios also indicate the time that the conversion between low and high marsh happens. The low and high marsh in the parabola is colored in blue and red and the arrow demonstrates how high marsh (red) becomes productive (green) and then is converted into low marsh (blue).

### 3. Results

The results of the hydrodynamic simulations include validation, vegetation productivity, species change, and migration possibility, in addition to marsh vulnerability index maps.

#### 3.1. Hydrodynamic Model Validation and Outputs

Simulated astronomic tides were validated by comparing modeled and observed water levels from a 14-day tidal resynthesis and during 20–30 April 2002. The resynthesized simulated water levels compare well in amplitude and phase to the resynthesized water levels based on measured data at all three NOAA water level gauges (left column of Figure 4). The Plum Island, Merrimack River gauge had the largest RMSE of 14.71 cm (less than 4% of the tidal range), and the Plum Island South station had the smallest RMSE of 10.90 cm (less than 3% of the tide range). In addition, simulated water levels agreed with observations for 20–30 April 2002 at all three gauge locations (right column of Figure 4). Error statistics were not computed for these stations due to the non-homogeneous sampling interval of the gauge.

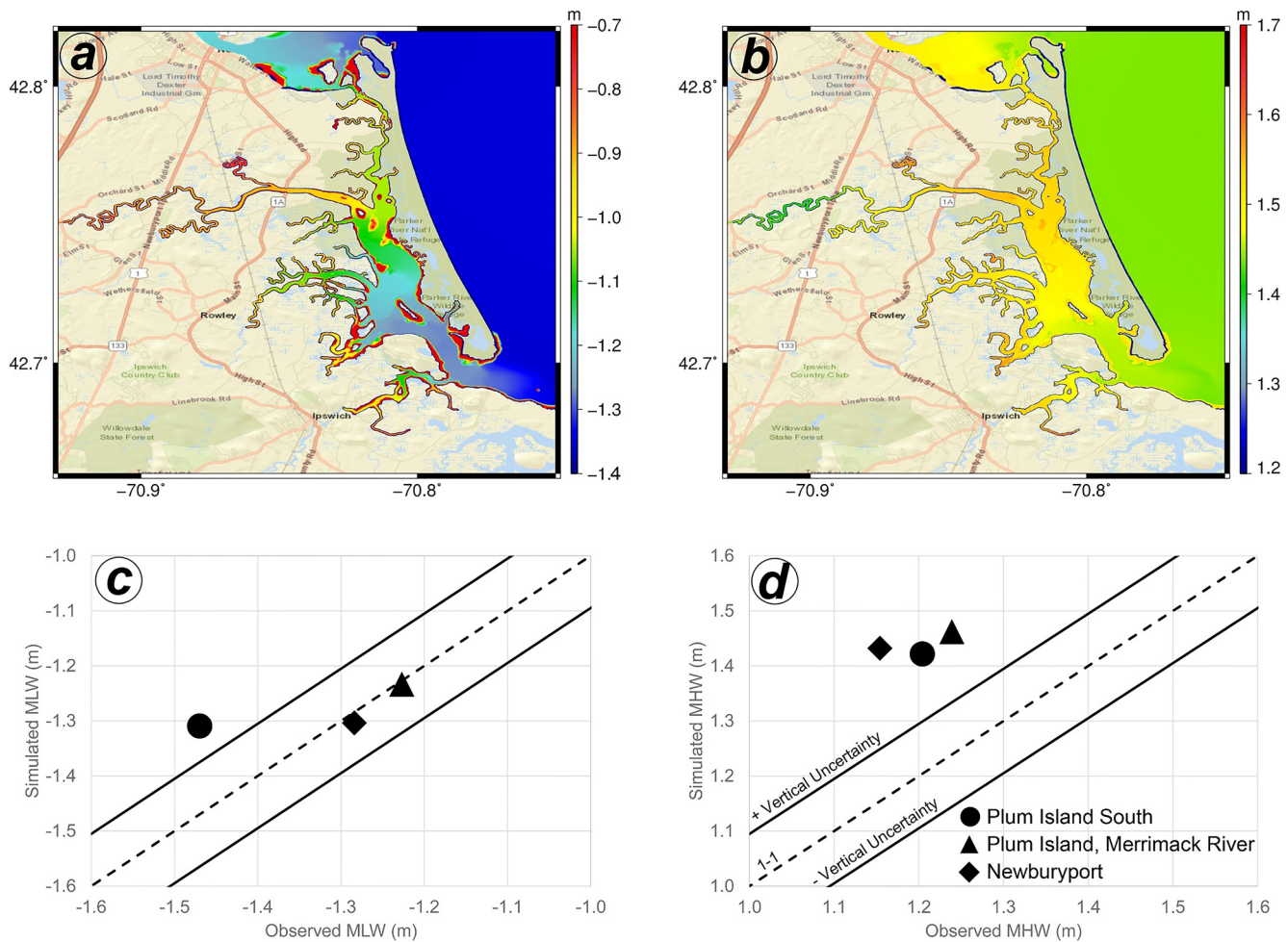


**Figure 5.** (a) Mean low water (MLW) and (b) mean high water (MHW) were computed from 90-day of simulated water levels. MLW and MHW validation (c and d) for the three National Oceanic and Atmospheric Administration (NOAA) National Ocean Service (NOS) tide gauges referenced from NAVD88. The dashed line is the 1-1 line, and the solid lines represent the vertical uncertainty of  $\pm 9.5$  cm reported by the NOAA VDatum tool (Hess, 2012; Parker et al., 2003).

Simulated MHW varies from 1.3 to 1.6 m NAVD88, and MLW varies from  $-1.3$  to  $-0.7$  m NAVD88 within the estuary (Figures 5a and 5b). Simulated MHW is generally over-predicted by an average of 0.24 m, which is 20% of the observed value (Figure 5d). This error in MHW was canceled out for marsh results with the same amount of error in elevation data due to lidar data error in the marsh system (Alizad, Medeiros, Foster-Martinez, & Hagen, 2020; K. Alizad, Medeiros, Morris, & Hagen, 2020). The average error of simulated MLW is 0.05 m, which is less than 4% of the observed value (Figure 5c). Since MLW does not have any role in biomass density formulation in PIE, the MLW error does not affect marsh results. It is important to note the limitations in this comparison. First, the NAVD88 datum was not reported by NOAA at these three gauge locations. The conversion of MSL to NAVD88 was using NOAA VDatum, which has a vertical uncertainty of 9.5 cm in this region (Hess, 2012). Second, the simulations were forced only by astronomic tides and do not include other factors that may alter total water levels such as wind, atmospheric pressure, density-driven effects, river inflow, and rainfall-runoff. Nonetheless, simulated MHW and MLW well represent the spatial patterns of MHW and MLW found within the estuary.

### 3.2. Simulated Projection Results

Modeled marsh productivity for present conditions (Figure 6a) was categorized by classifying biomass density by dividing them equally into low, medium, and high productivity (Figure 3a). The southern region of PIE has higher productivity than the northern section. The northern region consists of high marsh, particularly around



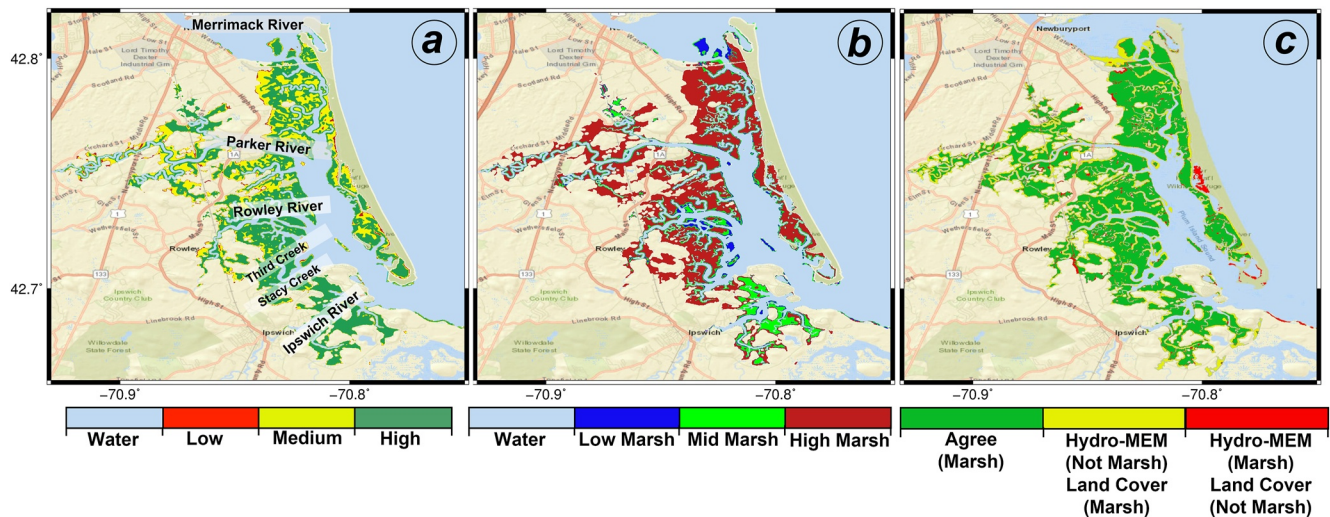


**Figure 6.** (a) Marsh productivity, (b) vegetation, and (c) validation maps for the current condition.

the Parker River. Low marsh is present within the center of PIE near the inlet of Rowley River, Third and Stacy Creeks, Roger and Holy Islands, and near the Merrimack River (Figure 6b). In addition, the mid marsh area between high and low marsh (colored as green in the vegetation map and as high productivity in the productivity map) is around the Ipswich River.

The simulated marsh coverage results were validated using National Wetland Inventory (NWI) data (Cowardin et al., 1979); the comparison map (Figure 6c) shows 67% of the modeled region is in agreement with the observations. Using Cohen's Kappa statistical method (Cohen, 1960; Landis & Koch, 1977; Monserud & Leemans, 1992), a Kappa value of 0.73 was computed, which suggests “substantial agreement” between Hydro-MEM and NWI data for marsh coverage (Landis & Koch, 1977).

Under three SLR projections, it was found that high marsh within the estuary increases in biomass productivity for the first 40 years (10%, 12%, and 13% for intermediate-low, intermediate, and intermediate-high SLR) (Figures 7 and 9a). Under the intermediate-low SLR scenario, the increase in productivity continued except for two islands within the PIE sound and one in the inlet of the Merrimack River (up to 13%) (Figures 7 and 9a). By the year 2100, under the intermediate-low scenario, changes to vegetation patterns start to emerge (Figure 8). The beginning of the major changes under the intermediate and intermediate-high SLR scenarios is around the year 2080 when the islands in the Merrimack River, the inlet of Rowley River, and Stacy and Third Creeks are projected to become mudflats. At the same time, land near the Ipswich River is predicted to lose productivity under the intermediate-high SLR scenario (Figure 7). Results for the year 2100 show a vast productive marsh area convert to mudflats and low productivity marsh under the intermediate-high SLR scenario (22% drop from 2080 to 2100 and 12% drop from 2020) (Figure 9a), whereas under the intermediate-low (13%) and intermediate SLR scenario (10%), the high productivity marsh compared to 2020 expands (Figure 9a). It is critical to combine this increase in marsh productivity under the intermediate and intermediate-low SLR scenarios with vegetation maps (Figure 8) to better understand the SLR effects on the PIE marsh system.

The intermediate-low SLR scenario resulted in minor changes in the species coverage between the three SLR scenarios (Figure 8). The percent coverage of vegetation through time (Figure 9b) for the intermediate-low SLR scenario also indicates that the low marsh and mid marsh area increased 3% and 5%, respectively. In contrast, high marsh reduced by 2% by the year 2100 compared to the current condition. More pronounced changes can be seen with the intermediate and intermediate-high SLR scenarios where high marsh was replaced by the low marsh and the low marsh region became mudflats in both scenarios. The analysis of vegetation coverage showed a 22% and 19% increase in the low marsh region under the intermediate and intermediate-high SLR scenarios, respectively. This gain in the low marsh is due to an 18% loss of high marsh area for both SLR scenarios and its conversion to low marsh. The conversion of high marsh to low marsh is projected to occur gradually from 2040 until 2080. During this time, the percent coverage of the mid marsh to low marsh is accelerated (Figures 8



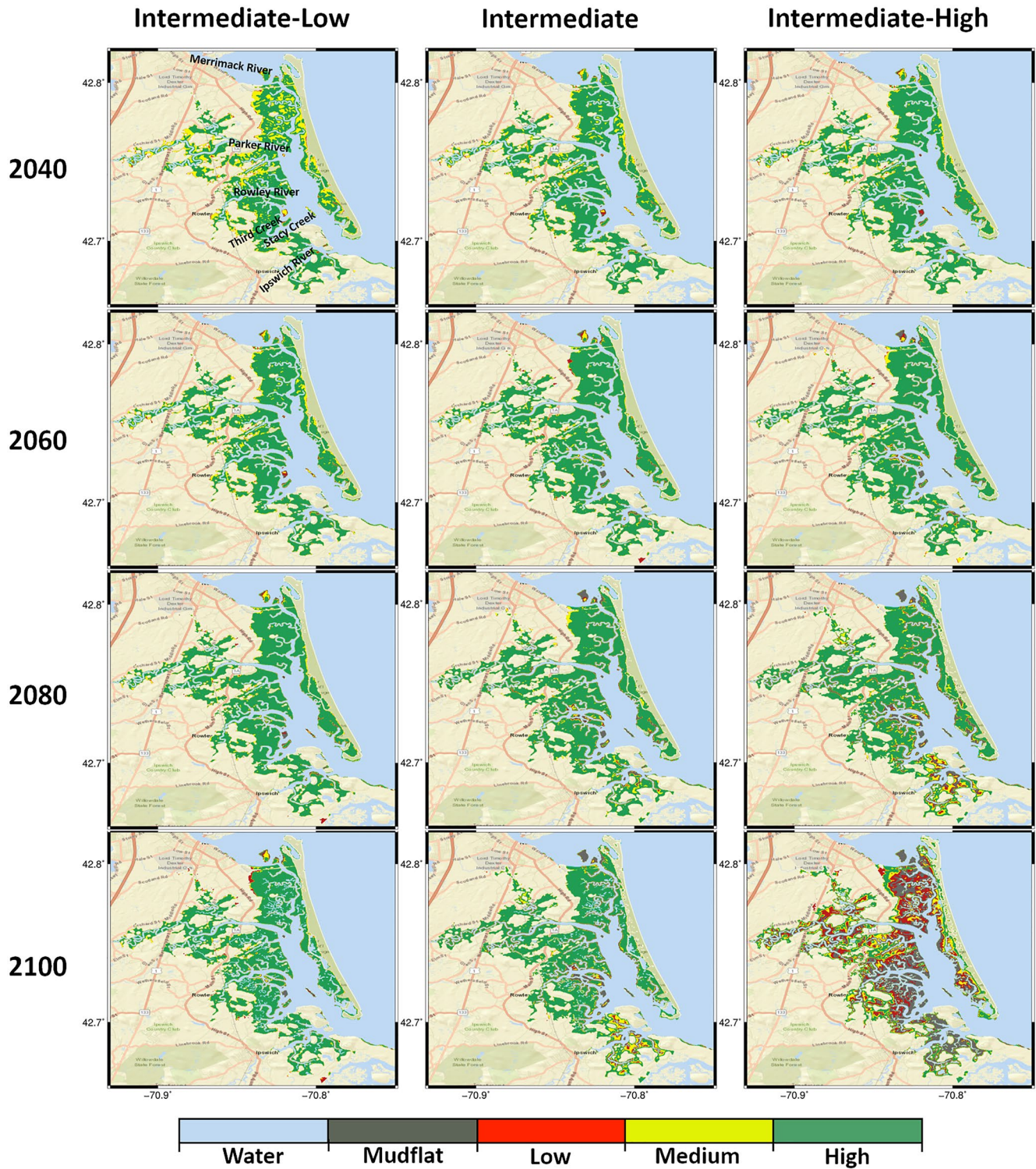


**Figure 7.** Marsh productivity projection maps. The columns show three sea-level rise (SLR) scenarios projections, and the rows demonstrate different years. The gray color shows mudflat regions and red, yellow, and green indicate low, medium, and high productivity areas, respectively.

and 9b). The same increase in the mid marsh coverage percentage was calculated from the year 2040–2080 under the intermediate-high SLR scenario. This SLR scenario was estimated to impact 16% of the low marsh area through conversion to mudflats with more concentration in the southern part from 2080 to 2100.



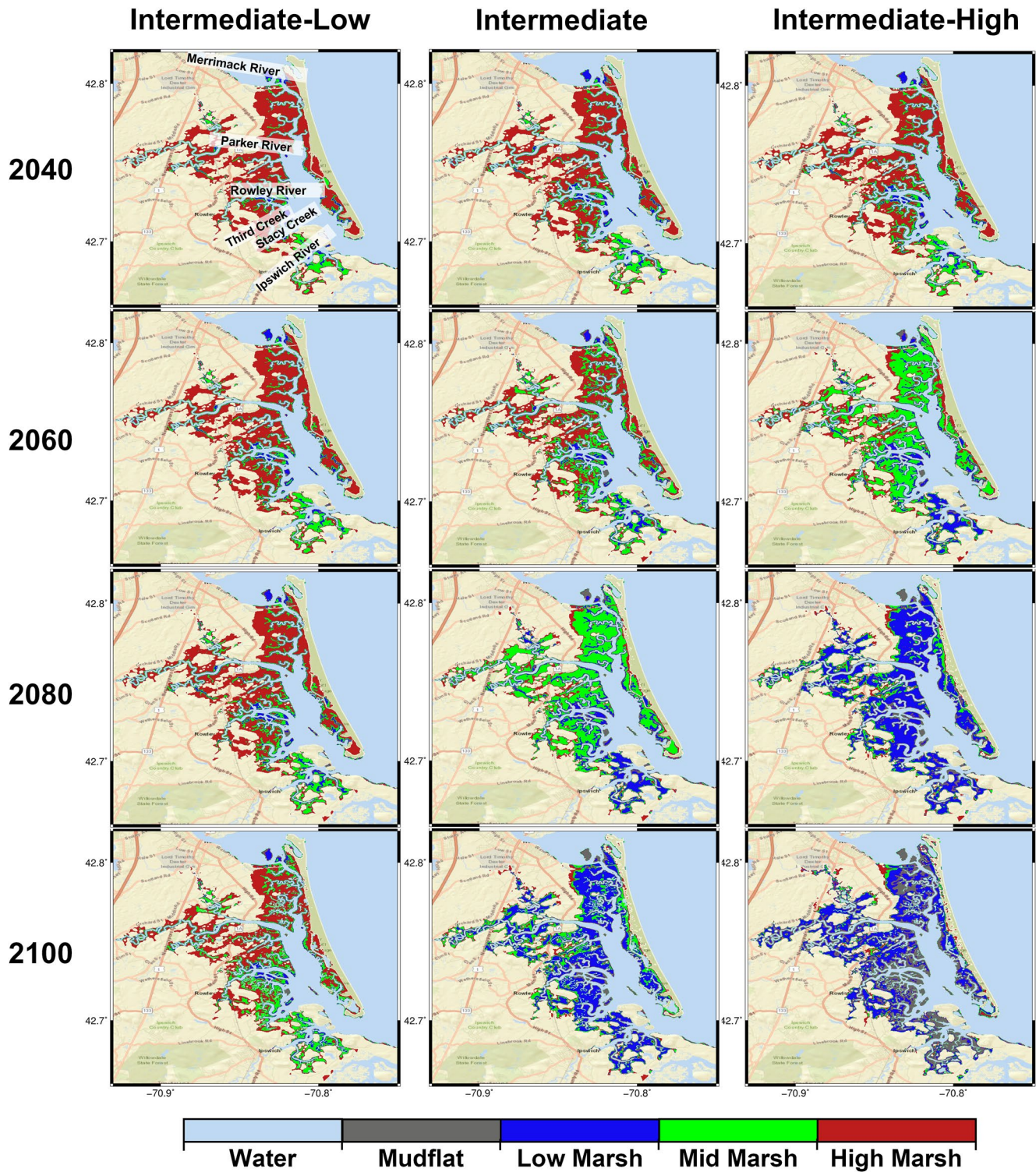


**Figure 8.** Marsh vegetation projection maps. The columns show three sea-level rise (SLR) scenarios projections and rows demonstrate different years. The gray color shows mudflat regions and blue, green, and red indicate low marsh, mid marsh, and high marsh regions, respectively.

A marsh vulnerability index was developed from the Hydro-MEM results for PIE. The marsh vulnerability index is defined as the existence of a marsh area in response to SLR over a specific time period under each SLR scenario. If the marsh is expected to disappear (i.e., convert to a mudflat or drown out) in 10 or fewer years, the

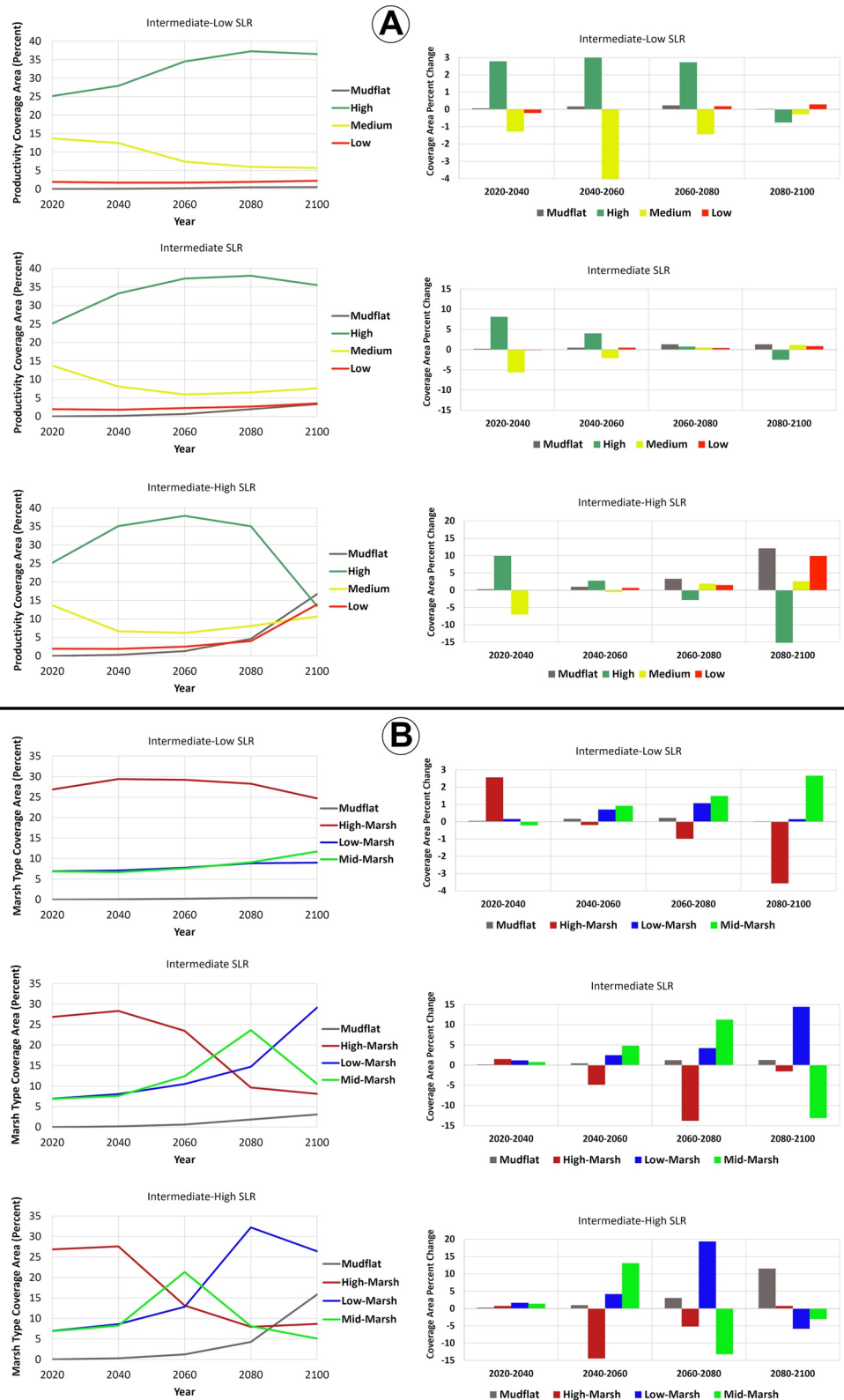


**Figure 9.** (a) Marsh productivity coverage area percentage and (b) marsh vegetation type area percentage with respect to the whole land in the model domain and (a) percentage change of each marsh productivity/mudflat and (b) vegetation type/mudflat in a 20-year time period for the three sea-level rise (SLR) scenarios.



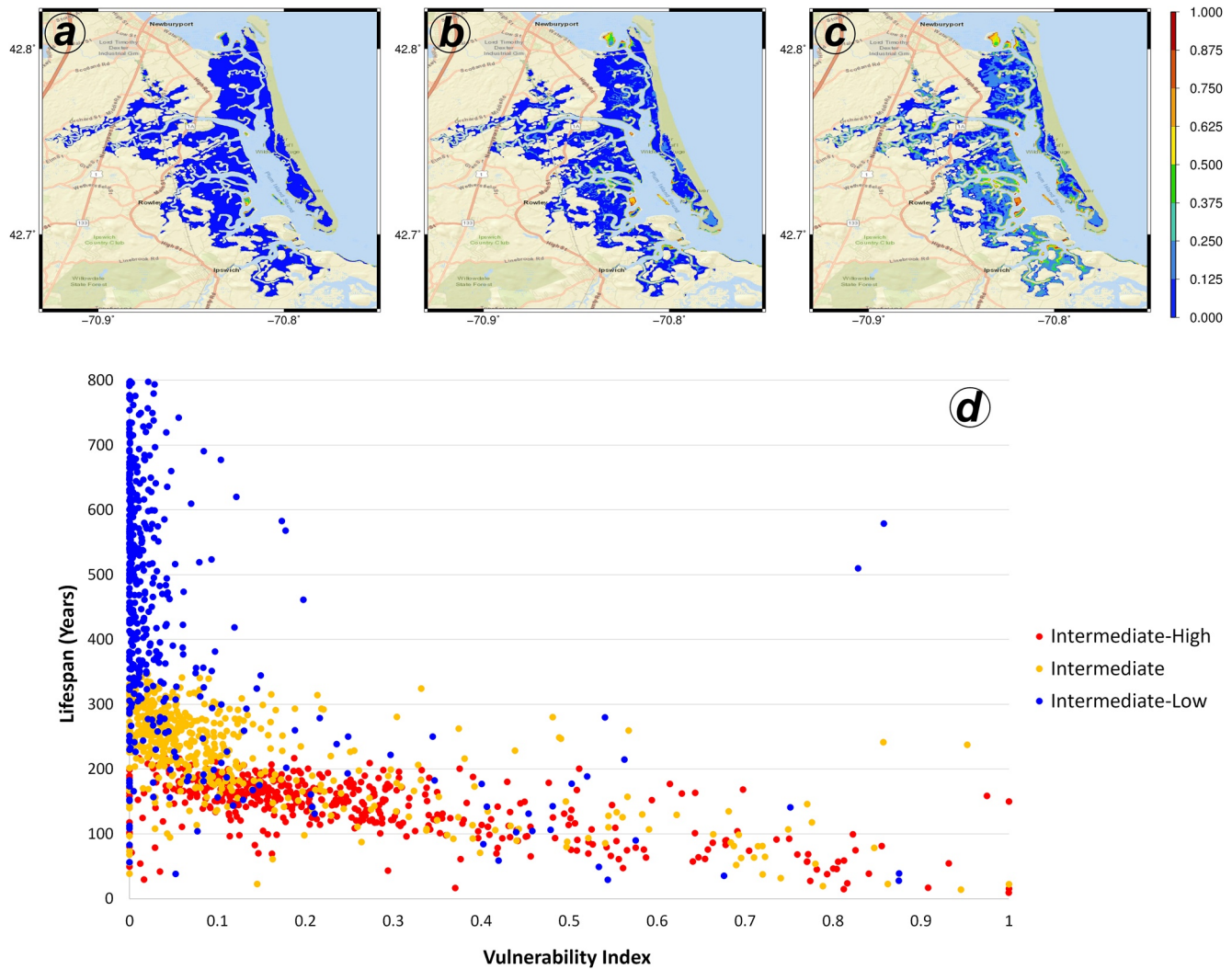


**Figure 10.** (a) Marsh vulnerability index for intermediate-low, (b) intermediate, (c) and intermediate-high sea-level rise (SLR) scenarios based on their vulnerability to that specific SLR. Warmer colors indicate higher vulnerability, cooler colors indicate lower vulnerability. The graph (d) shows the vulnerability index data versus the sediment-based marsh lifespan from another study in the same region by Ganju et al. (2020) for the three SLR scenarios.

vulnerability index is one (high vulnerability). If the estimation implies the marsh disappears in 80 years, its value is zero (low vulnerability). Therefore, for the marsh that is projected to become mudflat in 40 years, the vulnerability index is 0.5 (Figures 10a–10c). The marsh system in PIE showed low vulnerability under intermediate-low and intermediate SLR scenarios, except in the low marsh regions for the current conditions, which disappear faster than the high marsh regions (Figure 6b). However, the analysis for this marsh system under the intermediate-high SLR scenario indicated a higher vulnerability compared to the other two scenarios in the southern part of the estuary. A comparison between the vulnerability index and sediment-based lifespan parameter from studies by Ganju et al. (2020) and Ganju et al. (2017) demonstrated a correlation between these two parameters (Figure 10d). Sediment-based lifespan is defined as the time that marsh has its required sediment budget to keep itself in equilibrium with sea level. The comparison shows a higher vulnerability for the marshes with lower lifespans and vice versa. In other words, there is an inverse relation between vulnerability index from Hydro-MEM and lifespan defined by Ganju et al. (2017, 2020). The intermediate-low SLR marsh vulnerability scenario showing most of the marshes with vulnerability index value of zero was correlated with a higher lifespan; the higher vulnerability index under the higher SLR scenarios was correlated with a lower lifespan.

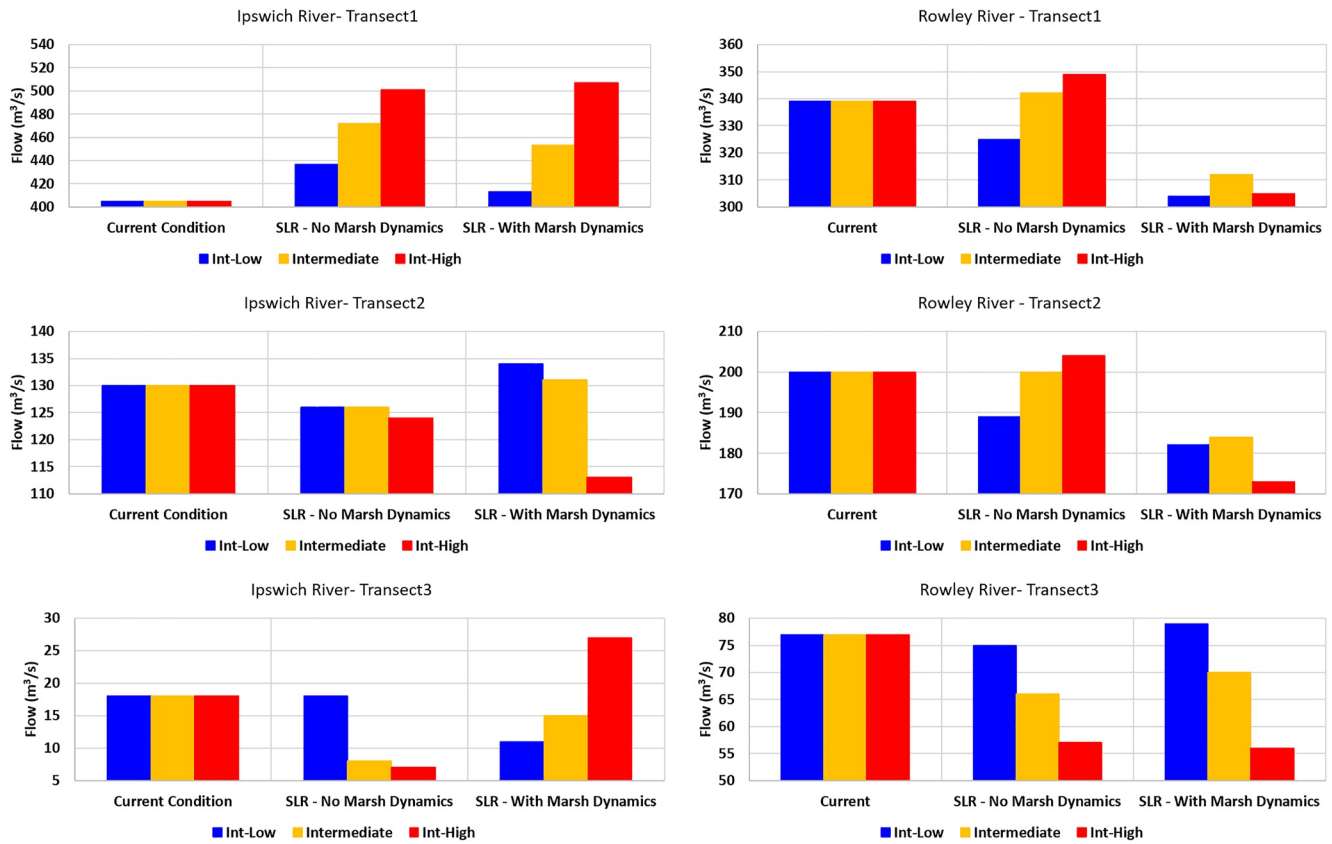


**Figure 11.** Tidal flow change under three sea-level rise (SLR) scenarios in three transects (transect 1 shown in the first row is in the inlet, transect 2 shown in the second row is in the middle of the river, transect 3 shown in the third row is the transect in upland) in the Ipswich and Rowley Rivers for the current condition, SLR without marsh feedback, and SLR with marsh feedback simulations.

### 3.3. Tidal Flow Dependency to Marsh Dynamics

To emphasize the critical role of integrated modeling and including hydrodynamic and biological feedbacks, simulations for the current conditions of SLR without marsh feedback, and SLR with marsh feedback were compared and contrasted. The SLR without marsh feedback simulation does not include marsh platform accretion, marsh productivity, and migration to higher lands and their effect on bottom friction. However, the SLR with marsh feedback simulation considers all of these changes for hydrodynamic simulations. The change in maximum tidal flow (herein called tidal flow) under the three SLR scenarios was assessed in Ipswich and Rowley Rivers across three cross-shore transects (Figure 1) located in (a) the inlet, (b) middle of the river, which has the highest productivity and coverage of marsh vegetation, and (c) the upper narrower part of the river farther from the marsh system.

The Ipswich River demonstrated different behaviors in tidal flow among all three transects (Figure 11). An increase in flow from 1% to 26% with and without capturing marsh dynamics in hydrodynamic modeling was observed across Transect 1. Transect 2 of Ipswich River results in reduced flow up to 5% for the SLR without marsh feedback simulation. In contrast, an increase of up to 3% for the SLR with marsh feedback simulation is shown for the intermediate-low and intermediate scenarios and a decrease of 13% for the intermediate-high SLR scenario. Transect 3 showed constant flow under no marsh dynamics simulation and decreased flow under the marsh dynamics simulation for the intermediate-low SLR scenario (0% for no marsh feedback and 39% drop for with marsh feedback) and a decrease in flow for both simulations under the intermediate SLR scenarios (17% for no marsh feedback and 55% for with marsh feedback). However, this transect simulation indicated two divergent flow trends for the intermediate-high SLR (61% drop for no marsh feedback and 50% increase for with marsh feedback).

For the Rowley River transects, flow at the first two transects under the intermediate and intermediate-high SLR scenarios for the SLR without marsh feedback simulation increased (1%–3%) or remained constant whereas it decreased for the intermediate-low SLR scenario (4%–6%). This trend was also seen at transect 3 for all three sea-level changes (3%, 14%, and 26% for the intermediate-low, intermediate, and intermediate-high SLR, respectively). Employing marsh dynamics (SLR with marsh feedback simulation) presented a drop in the flow for the first two transects (8%–14%) and an increased flow (3%) for the third transect under the intermediate-low SLR scenario. Details on the trends and how marsh dynamics affect tidal flow will be explained in the following section.

## 4. Discussion

It is important to note that this study is only considering the long-term (decadal to century-scale) future changes in astronomic tides under SLR and the resulting impacts on marsh productivity and therefore does not consider other short-term pulses that may be impactful in seasonal or annual marsh system change (e.g., extreme storms and resulting changes in sediment availability, marsh edge erosion due to waves). The PIE mesotidal estuary is better suited to withstand SLR than the microtidal estuaries in the Gulf of Mexico and the Mediterranean Sea (Alizad, Hagen, Morris, Medeiros, et al., 2016; Alizad et al., 2018; Day et al., 1995, 2011; Osland et al., 2017).

### 4.1. Marsh System Dynamics

The main drivers of the variations in MLW and MHW, especially from south to north of the estuary and along the creeks are the dominant ebb regime combined with the topographic, shoreline, and creek geometric variations. These hydrodynamic changes coupled with vegetation dynamics and sediment transport in the system demonstrate marsh productivity transition from low to medium to high in the estuary. Although winds drive seasonal changes in water levels, these effects are likely to average out over the long term and therefore these were not included in the model. In the current condition, higher water levels in the northern part of the estuary resulted in lower productivity compared to the southern part. However, the dominant vegetation is high marsh (*S. patens*) (Figures 5, 6a and 6b). In the mid marsh near the Ipswich River, the combination of low elevation and lower water level achieves the optimal relative depth for marsh biomass production. This section of the marsh is in the transition between high and low marsh with high productivity on the low marsh side (Figure 3). Since the current marsh system at PIE has a limited source of estuarine sediment, which will be influenced by SLR by an increase in ebb-dominated currents (Zhang et al., 2020), it is critical to investigate future patterns of the PIE marsh system, including both organic and inorganic sources for marsh elevation increase.

Hydro-MEM projections indicated adequate elevation change due to marsh platform accretion that keeps PIE marshes in equilibrium with SLR (Morris et al., 2002) for the first 40 years under all scenarios. Topography and vertical growth distribution explain the creation of mudflats and loss in productivity near the Ipswich River after the year 2080 under the intermediate-high SLR scenarios (Figures 1c and 3). The relative elevation (D) increases by increasing sea level, and the equilibrium point will move to the far-right side of the parabola, corresponding to low productivity and conversion to mudflat at the terminus of the parabola (Figure 3a). Under the intermediate-low and intermediate SLR for the same time frame, the marsh equilibrium moves from the left side of the curve toward the optimum elevation, resulting in the high productivity regions (Figure 3a).

In addition to the productivity changes, it is critical to understand how increasing sea level can shift the vegetation from high marsh to low marsh. This is demonstrated by examining the region near the Ipswich River shown as a mid-marsh under the current condition and the lower elevations around them. These lands are optimal areas on the left side of the mid marsh in the parabola (suboptimal side of the growth curve) (Figure 3b). The conversion of the mid marsh to low marsh under the intermediate and intermediate-high SLR scenarios in the year 2060 and 2080 (Figure 9b), indicates how vast, low lying areas in the northern part of the estuary move from the suboptimal side of the growth depth range to the superoptimal side (Figure 3b).

Although this marsh productivity analysis demonstrates marsh loss and mudflat creation under the intermediate-high SLR scenario (up to 17% of the domain land) (Figure 9a), results show marsh expansion and migration. However, the high elevation gradient around the current marsh regions limits the potential for migration, especially compared to projections of marsh migration in microtidal systems like the Gulf of Mexico (Alizad et al., 2018). These pronounced impacts of the higher SLR scenarios on the PIE marsh system demonstrated in



this research agree with the other research findings in the New England marsh species (Morris et al., 2013; Orson et al., 1998; Warren & Niering, 1993). Due to the higher tide range, the topography, and productive vegetation, the system can adapt more easily to SLR than microtidal marsh systems; this is reflected in the low vulnerability index for the two lower SLR scenarios. However, under the intermediate-high SLR scenario, there are more vulnerable regions, particularly around the Ipswich River and in some areas around the Rowley River, that may be considered for future restoration or designation of protected lands.

#### 4.2. Vulnerability Assessment

The comparison between the vulnerability index and sediment-based lifespan parameter (Ganju et al., 2017, 2020) (Figure 10d) indicates that under the intermediate-low SLR, zero vulnerability (most of the map) is correlated with a very high lifespan in Ganju et al. (2020) research. The inverse correlation between the Hydro-MEM vulnerability index for higher SLR scenarios and lifespan illustrates internal consistency. The fundamental agreement between these two approaches arises from marsh elevation, as higher elevation marshes in the Hydro-MEM framework are more optimal in the tidal level-biomass relation. In the sediment-based lifespan framework, lifespan is increased with more elevation and, therefore, more sediment stored above MSL. Second, as elevation and unvegetated to vegetated ratio (UVVR) are correlated in this region (Ganju et al., 2020), lifespan increases in tandem with lower UVVR. This suggests that two different approaches, one based on tide level-elevation-biomass formulations and another based on sediment storage and elevation capital, give similar results from a vulnerability perspective. Considering all the complexities included in the Hydro-MEM approach compared to the Ganju et al. (2017, 2020) sediment-based approach, the agreement on vulnerable zones helps coastal managers with informed decisions on priorities for the marsh system in this estuary.

#### 4.3. Landscape Effects on Flow Dynamics

Tidal flow analysis for the two main creeks in the south and north part of the estuary demonstrated the feedbacks between vegetation and hydrodynamics, emphasizing the need for integrated modeling approaches. The first transect in the inlet of Ipswich River is located at the sound entrance, and when the sea level rises without considering changes to the marsh, tidal flow increases. When accounting for the marsh dynamics, tidal flows were reduced compared to the scenario results that did not include marsh feedback.

Transect 2 is further upstream, where the marsh has the opportunity to impede the flow. In this part of the river, when the sea level in the model increased and elevation and friction were unchanged (SLR without marsh feedback simulation), higher water levels inundated the marsh and lowlands, and flow in the creek decreased and the same process happens for the transect 3. Employing Hydro-MEM (SLR with marsh feedback simulation) in the intermediate-low and intermediate SLR showed how accretion and increasing friction maintained water in the creek rather than dispersing it onto low elevation lands. Consequently, the tidal flow increased but transect 3 is far enough from the inlet to experience some drop in the flow. However, in the SLR with marsh feedback simulation for the intermediate-high SLR scenario (Figure 7), marshlands became mudflats which reduced friction and, as a result, allowed more water to flow onto nearby low-lying areas, which decreased flow in the creek in the second transect but increased in the third transect since it is far from marshlands (Figure 11).

Flow in the north Rowley River was shown to be more affected by the marsh system. The transect selected in the inlet is also surrounded by marsh. For this transect, the Intermediate-low SLR inundated surrounding lowlands before reaching the Rowley River, and tidal flow in the inlet decreased with increasing sea level. In the other SLR scenarios, higher sea levels inundated surrounding lowlands and increased the flow in the inlet of the Rowley River. However, by applying accretion, friction change, and marsh migration using Hydro-MEM modeling (SLR with marsh feedback simulation) for the intermediate and intermediate-high SLR, the dynamics of the system changed. The flow of water moves with less resistance in the estuary due to mudflat creation (lower bottom friction) and marsh migration to higher lands (less dense marsh grasses and lower bottom friction) and in turn, the flow in the inlet of the Rowley River was estimated to decrease with increasing sea level. The same trend for the second transect was projected although it was not affected as much by the marsh system dynamics. The third transect location is upstream with productive marsh under the intermediate-low SLR scenario and consequently, the flow at this transect showed a slight increase. However, under the higher SLR scenarios, the effects

of low marsh productivity, mudflat creation, as well as marsh migration as described for the inlet of this creek, reduced the flow.

Future work in this estuary could focus on doing hindcast simulation using soil core data and sea-level change in the past century and using the projections to generate UVVR index for this region. In addition, the next updates in Hydro-MEM include sediment transport and bathymetric changes module that could be applied in this estuary in the future. Due to hydrodynamic model capabilities in modeling large study regions, Hydro-MEM could be used on regional scale by advancing MEM general spatially-varying parametrization. The preliminary updated Hydro-MEM with spatial parametrization of MEM was tested on a regional scale at Apalachicola-Big-Bend (ABB) region (Alizad, Medeiros, Foster-Martinez, & Hagen, 2020; K. Alizad, Medeiros, Morris, & Hagen, 2020), and could be finalized and tested in other regions in the near future.

## 5. Conclusion

This research demonstrated the vulnerability of the PIE marsh system to three SLR scenarios. Updates to Hydro-MEM were applied that include mudflat generation module, updated marsh platform accretion formulation, vegetation change, and vulnerability index components in addition to all previously established coupled hydrodynamic-marsh features. This integrated model simulated vegetation change from high marsh (*S. patens*) to low marsh (*S. alterniflora*) in all three SLR scenarios, which were more extreme under the higher rates of SLR. Mudflats were projected to develop in low marsh areas under the higher SLR scenarios, with some creek expansion and limited marsh migration to higher lands due to steep topography at PIE. These changes were more pronounced in the middle and southern parts of the estuary where lower lands, as well as low marsh, are present. As indicated by the vulnerability index, these lands were the most vulnerable regions under the intermediate-high SLR scenario and would likely benefit from restoration activities in the future. One of the main conclusions of this research is the critical role of integrated modeling for the densely vegetated regions due to the nonlinear effects of vegetation dynamics on hydrodynamics. This research illustrated how the maximum tidal flow in two main creeks of this system responds differently to rising sea level because of neighboring vegetation dynamic effects, that would not be accounted for with simplistic SLR modeling.

## Acknowledgments

This research is partially funded under Award No. NA16NOS4780208 from the National Oceanic and Atmospheric Administration (NOAA) Center for Sponsored Coastal Ocean Research (CSCOR), and awards EAR1660502 and OCE-1637630 from the NSF, and the Louisiana Sea Grant Laborde Chair. The computations for the hydrodynamic model simulations were performed using the Extreme Science and Engineering Discovery Environment (XSEDE), which is supported by the NSF Grant No. ACI-1053575 (Townsend et al., 2014), and High-Performance Computing at Louisiana State University (LSU) and the Louisiana Optical Network Initiative (LONI). The authors would like to extend our thanks appreciation to Kate Ackerman and Neil Ganju who provided geospatial analysis for comparing the vulnerability index with the sediment-based lifespan, and Plum Island Ecosystem LTER staff, for their help and support. The statements and conclusions do not necessarily reflect the views of Louisiana Sea Grant, NSF, NOAA, XSEDE, LSU, LONI, Plum Island Ecosystem LTER, or their affiliates. Any use of trade, firm, or product names is for descriptive purposes only and does not imply endorsement by the U.S. Government.

## Data Availability Statement

Marsh outputs have been published in the Northeast Conservation Planning Atlas (Northeast CPA): <https://nalcc.databasin.org/galleries/e9580baf3350425a9eb309a4f4029766/> and bathymetric data used in this study were obtained at <http://eco37.mbl.edu/FVCOM/PIE-FVCOM.html>, and more specifically, the direct download link for this data is [http://eco37.mbl.edu/FVCOM/PIE\\_Bathymetry\\_V4\\_LatLong.zip](http://eco37.mbl.edu/FVCOM/PIE_Bathymetry_V4_LatLong.zip).

## References

- Alizad, K., Hagen, S. C., Medeiros, S. C., Bilskie, M. V., Morris, J. T., Balthis, L., & Buckel, C. A. (2018). Dynamic responses and implications of coastal wetlands and the surrounding regions under sea level rise. *PLoS One*, *13*(10), e0205176. <https://doi.org/10.1371/journal.pone.0205176>
- Alizad, K., Hagen, S. C., Morris, J. T., Bacopoulos, P., Bilskie, M. V., Weishampel, J., & Medeiros, S. C. (2016). A coupled, two-dimensional hydrodynamic-marsh model with biological feedback. *Ecological Modeling*, *327*, 29–43. <https://doi.org/10.1016/j.ecolmodel.2016.01.013>
- Alizad, K., Hagen, S. C., Morris, J. T., Medeiros, S. C., Bilskie, M. V., & Weishampel, J. F. (2016). Coastal wetland response to sea-level rise in a fluvial estuarine system. *Earth's Future*, *4*(11), 483–497. <https://doi.org/10.1002/2016EF000385>
- Alizad, K., Medeiros, S. C., Foster-Martinez, M. R., & Hagen, S. C. (2020). Model sensitivity to topographic uncertainty in Meso- and microtidal marshes. *Ieee Journal of Selected Topics in Applied Earth Observations and Remote Sensing*, *13*, 807–814. <https://doi.org/10.1109/JSTARS.2020.2973490>
- Alizad, K., Medeiros, S. C., Morris, J. T., & Hagen, S. C. (2020). Northwest Florida coastal wetland response to sea-level rise using Apalachicola-big-bend (ABB) hydrodynamic model. In *Paper presented at AGU fall meeting abstracts*. Retrieved from <https://ui.adsabs.harvard.edu/abs/2020AGUFMOS008.02A>
- Bacopoulos, P., Tritinger, A. S., & Dix, N. G. (2019). Sea-level rise impact on salt marsh sustainability and migration for a subtropical estuary: GTMNERR (Guana tomatato Matanzas national estuarine research reserve). *Environmental Modeling & Assessment*, *24*(2), 163–184. <https://doi.org/10.1007/s10666-018-9622-6>
- Barbier, E. B., Georgiou, I. Y., Enchelmeyer, B., & Reed, D. J. (2013). The value of wetlands in protecting southeast Louisiana from hurricane storm surges. *PLoS One*, *8*(3), e58715. <https://doi.org/10.1371/journal.pone.0058715>
- Bilskie, M. V., & Hagen, S. C. (2013). Topographic accuracy assessment of bare Earth Lidar-derived unstructured meshes. *Advances in Water Resources*, *52*, 165–177. <https://doi.org/10.1016/j.advwatres.2012.09.003>
- Bilskie, M. V., Hagen, S. C., Alizad, K., Medeiros, S. C., Passeri, D. L., Needham, H. F., & Cox, A. (2016). Dynamic simulation and numerical analysis of hurricane storm surge under sea level rise with geomorphologic changes along the northern Gulf of Mexico. *Earth's Future*, *4*(5), 177–193. <https://doi.org/10.1002/2015EF000347>

- Boon, J. D., III, & Kiley, K. P. (1978). *Harmonic analysis and tidal prediction by the method of least squares: A user's manual*. Virginia Institute of Marine Science, William & Mary. <https://doi.org/10.21220/V5PF2T>
- Buchsbaum, R. N., Deegan, L. A., Horowitz, J., Garritt, R. H., Giblin, A. E., Ludlam, J. P., & Shull, D. H. (2009). Effects of regular salt marsh haying on marsh plants, algae, invertebrates and birds at Plum Island sound, Massachusetts. *Wetlands Ecology and Management*, 17(5), 469–487. <https://doi.org/10.1007/s11273-008-9125-3>
- Buth, G. J. C., & Voesenek, L. A. C. J. (1987). Decomposition of standing and fallen litter of halophytes in a Dutch salt marsh. In A. H. L. Huiskes, C. W. P. M. Blom, & J. Rozema (Eds.), *Vegetation between land and sea: Structure and processes* (pp. 146–162). Springer Netherlands.
- Cohen, J. (1960). A coefficient of agreement for nominal scales. *Educational and Psychological Measurement*, 20(1), 37–46. <https://doi.org/10.1177/001316446002000104>
- Costanza, R., Pérez-Maqueo, O., Martinez, M. L., Sutton, P., Anderson, S. J., & Mulder, K. (2008). The value of coastal wetlands for hurricane protection. *AMBIO: A Journal of the Human Environment*, 37(4), 241–248. [https://doi.org/10.1579/0044-7447\(2008\)37\[241:TVOCWF\]2.0.CO;2](https://doi.org/10.1579/0044-7447(2008)37[241:TVOCWF]2.0.CO;2)
- Cowardin, L. M., Carter, V., Golet, F. C., & LaRoe, E. T. (1979). *Classification of wetlands and deepwater habitats of the United States rep.* US Department of the Interior, US Fish and Wildlife Service.
- Crosby, S. C., Sax, D. F., Palmer, M. E., Booth, H. S., Deegan, L. A., Bertness, M. D., & Leslie, H. M. (2016). Salt marsh persistence is threatened by predicted sea-level rise. *Estuarine, Coastal and Shelf Science*, 181, 93–99. <https://doi.org/10.1016/j.ecss.2016.08.018>
- Daiber, F. (1977). Salt marsh animals: Distributions related to tidal flooding, salinity and vegetation. In V. J. Chapman (Ed.), *Wet coastal ecosystems* (pp. 79–108). Elsevier Scientific Publishing Company.
- D'Alpaos, A., Lanzoni, S., Marani, M., & Rinaldo, A. (2007). Landscape evolution in tidal embayments: Modeling the interplay of erosion, sedimentation, and vegetation dynamics. *Journal of Geophysical Research*, 112(F1), F01008. <https://doi.org/10.1029/2006JF000537>
- Darby, F. A., & Turner, R. E. (2008). Below- and aboveground *Spartina alterniflora* production in a Louisiana salt marsh. *Estuaries and Coasts*, 31(1), 223–231. <https://doi.org/10.1007/s12237-007-9014-7>
- Day, J., Ibáñez, C., Scarton, F., Pont, D., Hensel, P., Day, J., & Lane, R. (2011). Sustainability of mediterranean deltaic and lagoon wetlands with sea-level rise: The importance of river input. *Estuaries and Coasts*, 34(3), 483–493. <https://doi.org/10.1007/s12237-011-9390-x>
- Day, J., Pont, D., Hensel, P., Ibáñez, C., & Ibanez, C. (1995). Impacts of sea-level rise on deltas in the Gulf of Mexico and the mediterranean: The importance of pulsing events to sustainability. *Estuaries*, 18(4), 636–647. <https://doi.org/10.2307/1352382>
- Fagherazzi, S., Kirwan, M. L., Mudd, S. M., Guntenspergen, G. R., Temmerman, S., D'Alpaos, A., et al. (2012). Numerical models of salt marsh evolution: Ecological, geomorphic, and climatic factors. *Reviews of Geophysics*, 50(1), RG1002. <https://doi.org/10.1029/2011RG000359>
- Forbrich, I., Giblin, A. E., & Hopkinson, C. S. (2018). Constraining marsh carbon budgets using long-term C burial and contemporary atmospheric CO<sub>2</sub> fluxes. *Journal of Geophysical Research: Biogeosciences*, 123(3), 867–878. <https://doi.org/10.1002/2017jg004336>
- Foster-Martinez, M. R., Alizad, K., & Hagen, S. C. (2020). Estimating wave attenuation at the coastal land margin with a GIS toolbox. *Environmental Modelling & Software*, 132, 104788. <https://doi.org/10.1016/j.envsoft.2020.104788>
- Friedrichs, C. T., & Perry, J. E. (2001). Tidal salt marsh morphodynamics: A synthesis. *Journal of Coastal Research*, 7–37. <https://doi.org/10.2307/25736162>
- Ganju, N. K., Defne, Z., & Fagherazzi, S. (2020). Are elevation and open-water conversion of salt marshes connected? *Geophysical Research Letters*, 47(3), e2019GL086703. <https://doi.org/10.1029/2019GL086703>
- Ganju, N. K., Defne, Z., Kirwan, M. L., Fagherazzi, S., D'Alpaos, A., & Carniello, L. (2017). Spatially integrative metrics reveal hidden vulnerability of microtidal salt marshes. *Nature Communications*, 8(1), 14156. <https://doi.org/10.1038/ncomms14156>
- Hagen, S., Morris, J., Bacopoulos, P., & Weishampel, J. (2013). Sea-level rise impact on a salt marsh system of the lower St. Johns River. *Journal of Waterway, Port, Coastal, and Ocean Engineering*, 139(2), 118–125. [https://doi.org/10.1061/\(ASCE\)WW.1943-5460.0000177](https://doi.org/10.1061/(ASCE)WW.1943-5460.0000177)
- Hess, K. (2012). *V DATUM manual for development and support of NOAA's vertical datum transformation tool, V DATUM*. Office of Coast Survey, National Geodetic Survey.
- Hodson, R. E., Christian, R. R., & Maccubbin, A. E. (1984). Lignocellulose and lignin in the salt marsh grass *Spartina alterniflora*: Initial concentrations and short-term, post-depositional changes in detrital matter. *Marine Biology*, 81(1), 1–7. <https://doi.org/10.1007/bf00397619>
- Hopkinson, C. S., Morris, J. T., Fagherazzi, S., Wollheim, W. M., & Raymond, P. A. (2018). Lateral marsh edge erosion as a source of sediments for vertical marsh accretion. *Journal of Geophysical Research: Biogeosciences*, 123(8), 2444–2465. <https://doi.org/10.1029/2017JG004358>
- Jansson, M., Rune, A., Hans, B., & Leonardson, L. (1994). Wetlands and lakes as nitrogen traps. *Ambio*, 23(6), 320–325.
- Jiang, L., Gerkema, T., Idier, D., Slangen, A. B. A., & Soetaert, K. (2020). Effects of sea-level rise on tides and sediment dynamics in a Dutch Tidal Bay. *Ocean Science*, 16(2), 307–321. <https://doi.org/10.5194/os-16-307-2020>
- Kadlec, R. H. (1999). Chemical, physical and biological cycles in treatment wetlands. *Water Science and Technology*, 40(3), 37–44. [https://doi.org/10.1016/S0273-1223\(99\)00417-5](https://doi.org/10.1016/S0273-1223(99)00417-5)
- Kidwell, D. M., Dietrich, J. C., Hagen, S. C., & Medeiros, S. C. (2017). An Earth's future special collection: Impacts of the coastal dynamics of sea level rise on low-gradient coastal landscapes. *Earth's Future*, 5(1), 2–9. <https://doi.org/10.1002/2016ef000493>
- Kirwan, M. L., & Guntenspergen, G. R. (2010). Influence of tidal range on the stability of coastal marshland. *Journal of Geophysical Research*, 115(F2). <https://doi.org/10.1029/2009jg001400>
- Kirwan, M. L., & Murray, A. B. (2007). A coupled geomorphic and ecological model of tidal marsh evolution. *Proceedings of the National Academy of Sciences*, 104(15), 6118–6122. <https://doi.org/10.1073/pnas.0700958104>
- Kirwan, M. L., Murray, A. B., Donnelly, J. P., & Corbett, D. R. (2011). Rapid wetland expansion during European settlement and its implication for marsh survival under modern sediment delivery rates. *Geology*, 39(5), 507–510. <https://doi.org/10.1130/g31789.1>
- Krone, R. (1987). A method for simulating historic marsh elevations. In *Paper presented at Coastal Sediments*. ASCE.
- Landis, J. R., & Koch, G. G. (1977). The measurement of observer agreement for categorical data. *Biometrics*, 33(1), 159–174. <https://doi.org/10.2307/2529310>
- Luettich, R., & Westerink, J. (2006). ADCIRC: A parallel advanced circulation model for oceanic, coastal and estuarine waters. In *Users manual for version 45.08*.
- Monserud, R. A., & Leemans, R. (1992). Comparing global vegetation maps with the kappa statistic. *Ecological Modelling*, 62(4), 275–293. [https://doi.org/10.1016/0304-3800\(92\)90003-W](https://doi.org/10.1016/0304-3800(92)90003-W)
- Morris, J. T. (1982). A model of growth responses by *Spartina alterniflora* to nitrogen limitation. *Journal of Ecology*, 70(1), 25–42. <https://doi.org/10.2307/2259862>
- Morris, J. T., Barber, D. C., Callaway, J. C., Chambers, R., Hagen, S. C., Hopkinson, C. S., et al. (2016). Contributions of organic and inorganic matter to sediment volume and accretion in tidal wetlands at steady state. *Earth's Future*, 4(4), 110–121. <https://doi.org/10.1002/2015EF000334>
- Morris, J. T., Sundareswar, P. V., Nietch, C. T., Kjerfve, B., & Cahoon, D. R. (2002). Responses of coastal wetlands to rising sea level. *Ecology*, 83(10), 2869–2877. [https://doi.org/10.1890/0012-9658\(2002\)083\[2869:rocwtr\]2.0.co;2](https://doi.org/10.1890/0012-9658(2002)083[2869:rocwtr]2.0.co;2)



- Morris, J. T., Sundberg, K., & Hopkinson, C. S. (2013). Salt marsh primary production and its responses to relative sea level and nutrients in estuaries at Plum Island, Massachusetts, and North Inlet, South Carolina, USA. *Oceanography*, 26(3), 78–84. <https://doi.org/10.5670/oceanog.2013.48>
- Mudd, S. M., Howell, S. M., & Morris, J. T. (2009). Impact of dynamic feedbacks between sedimentation, sea-level rise, and biomass production on near-surface marsh stratigraphy and carbon accumulation. *Estuarine, Coastal and Shelf Science*, 82(3), 377–389. <https://doi.org/10.1016/j.ecss.2009.01.028>
- Orson, R. A., Warren, R. S., & Niering, W. A. (1998). Interpreting sea level rise and rates of vertical marsh accretion in a southern New England tidal salt marsh. *Estuarine, Coastal and Shelf Science*, 47(4), 419–429. <https://doi.org/10.1006/ecss.1998.0363>
- Osland, M. J., Griffith, K. T., Larriviere, J. C., Feher, L. C., Cahoon, D. R., Enwright, N. M., et al. (2017). Assessing coastal wetland vulnerability to sea-level rise along the northern Gulf of Mexico Coast: Gaps and opportunities for developing a coordinated regional sampling network. *PLoS One*, 12(9), e0183431. <https://doi.org/10.1371/journal.pone.0183431>
- Parker, B., Hess, K., Milbert, D., & Gill, S. (2003). A national vertical datum transformation tool. *Sea Technology*, 44(9), 10–16.
- Parris, A., Bromirski, P., Burkett, V., Cayan, D., Culver, M., Hall, J., et al. (2012). Global sea level rise scenarios for the US national climate assessment. *Forestry Report*, 1–37.
- Partners, O. C. M. (2020). 2011 U.S. Geological Survey topographic LiDAR: LiDAR for the north east from 2010-06-15 to 2010-08-15. NOAA National Centers for Environmental Information.
- Passeri, D. L., Hagen, S. C., Medeiros, S. C., Bilskie, M. V., Alizad, K., & Wang, D. (2015). The dynamic effects of sea level rise on low-gradient coastal landscapes: A review. *Earth's Future*, 3(6), 159–181. <https://doi.org/10.1002/2015EF000298>
- Passeri, D. L., Hagen, S. C., Plant, N. G., Bilskie, M. V., Medeiros, S. C., & Alizad, K. (2016). Tidal hydrodynamics under future sea level rise and coastal morphology in the northern Gulf of Mexico. *Earth's Future*, 4(5), 159–176. <https://doi.org/10.1002/2015EF000332>
- Pennings, S. C., & Bertness, M. D. (2001). Salt marsh communities. In (Eds) M. D. Bertness, S. D. Gaines, & M. Hay (Eds.), *Marine community ecology* (pp. 289–316). Sinauer Associates.
- Raposa, K. B., Wasson, K., Smith, E., Crooks, J. A., Delgado, P., Fernald, S. H., et al. (2016). Assessing tidal marsh resilience to sea-level rise at broad geographic scales with multi-metric indices. *Biological Conservation*, 204, 263–275. <https://doi.org/10.1016/j.biocon.2016.10.015>
- Reed, D. J. (1995). The response of coastal marshes to sea-level rise: Survival or submergence? *Earth Surface Processes and Landforms*, 20(1), 39–48. <https://doi.org/10.1002/esp.3290200105>
- Rozas, L. P., Caldwell, P., & Minello, T. J. (2005). The fishery value of salt marsh restoration projects. *Journal of Coastal Research*, 37–50.
- Schmitt, C., Weston, N., & Hopkinson, C. (1998). Preliminary evaluation of sedimentation rates and species distribution in Plum Island estuary, Massachusetts. *The Biological Bulletin*, 195(2), 232–233. <https://doi.org/10.2307/1542855>
- Sweet, W., Kopp, R., Weaver, C., Obeysekera, J., Horton, R. M., Thieler, E. R., & Zervas, C. (2017). *Global and regional sea level rise scenarios for the United States rep. CO-OPS 083*. NOAA.
- Towns, J., Cockerill, T., Dahan, M., Foster, I., Gaither, K., Grimshaw, A., et al. (2014). XSEDE: Accelerating scientific discovery. *Computing in Science & Engineering*, 16(5), 62–74. <https://doi.org/10.1109/MCSE.2014.80>
- Vallino, J. J., & Hopkinson, J. C. S. (1998). Estimation of dispersion and characteristic mixing times in Plum Island sound estuary. *Estuarine, Coastal and Shelf Science*, 46(3), 333–350. <https://doi.org/10.1006/ecss.1997.0281>
- Warren, R. S., & Niering, W. A. (1993). Vegetation change on a northeast tidal marsh: Interaction of sea-level rise and marsh accretion. *Ecology*, 74(1), 96–103. <https://doi.org/10.2307/1939504>
- Wigand, C., Ardito, T., Chaffee, C., Ferguson, W., Paton, S., Raposa, K., et al. (2017). A climate change adaptation strategy for management of coastal marsh systems. *Estuaries and Coasts*, 40(3), 682–693. <https://doi.org/10.1007/s12237-015-0003-y>
- Wilson, J. O., Buchsbaum, R., Valiela, I., & Swain, T. (1986). Decomposition in salt marsh ecosystems: Phenolic dynamics during decay of litter of *Spartina alterniflora*. *Marine Ecology Progress Series*, 29(2), 177–187. <https://doi.org/10.3354/meps029177>
- Yoskowitz, D., Carollo, C., Pollack, J. B., Santos, C., & Welder, K. (2017). Integrated ecosystem services assessment: Valuation of changes due to sea level rise in Galveston Bay, Texas, USA. *Integrated Environmental Assessment and Management*, 13(2), 431–443. <https://doi.org/10.1002/ieam.1798>
- Zhang, X., Leonardi, N., Donatelli, C., & Fagherazzi, S. (2020). Divergence of sediment fluxes Triggered by sea-level rise will reshape coastal Bays. *Geophysical Research Letters*, 47(13), e2020GL087862. <https://doi.org/10.1029/2020GL087862>
- Zhao, L., Chen, C., Vallino, J., Hopkinson, C., Beardsley, R. C., Lin, H., & Lerczak, J. (2010). Wetland-estuarine-shelf interactions in the Plum Island sound and Merrimack River in the Massachusetts coast. *Journal of Geophysical Research*, 115(C10), 2009JC006085. <https://doi.org/10.1029/2009JC006085>